Diffusion-charge transfer characterization of a rotating cylinder electrode reactor used for the complete electrocatalytic removal of nitrate from water

Roger Oriol[a], José L. Nava[b,**], Enric Brillas[a], Ignasi Sirés[a,*]

[a] *Laboratori d'Electroquímica dels Materials i del Medi Ambient, Departament de Ciència de Materials i Química Física, Secció de Química Física, Facultat de Química, Universitat de Barcelona, Martí i Franquès 1-11, 08028 Barcelona, Spain.*

[b] *Departamento de Ingeniería Geomática e Hidráulica, Universidad de Guanajuato, Av. Juárez 77, Zona Centro, C.P 36000 Guanajuato, Mexico.*

Paper submitted for publication in the

Journal of Environmental Chemical Engineering

Corresponding author: * E-mail: i.sires@ub.edu (I. Sirés)

** E-mail: jlnm@ugto.mx (J.L. Nava)

Abstract

Groundwater nitrate contamination is an emerging threat in stressed regions under intensive farming although, lately, efforts to valorize such residues are highly encouraged. Here, electrochemical nitrate removal has been investigated as a versatile strategy for this purpose, using a reactor equipped with a cheap central Fe-based rotating cylinder electrode (RCE) as cathode and six concentric Ti|IrO_2 plates as anodes. The study of the effect of E_{cath} and rotational speed (ω) on NO_3^- electroreduction from a synthetic aqueous solution with high conductivity revealed the feasibility of complete nitrate removal, which only required 100-120 min at E_{cath} = -1.80 V vs Hg|Hg_2SO_4|sat. K_2SO_4 within the ω-range of 100-500 rpm. The concentration decays agreed perfectly with a first-order kinetics. NH_3 was accumulated as main product, being partly volatilized due to the quick solution alkalization, whereas NO_2^- was not found. Linear sweep voltammetries demonstrated the high electrocatalytic activity of carbon steel RCE as compared to inactive stainless steel. Koutecky-Levich analysis showed that the reduction process with carbon steel at E_{cath} from -1.80 V involved 8 electrons. The participation of H radical in the reduction mechanism was ascertained by electron paramagnetic resonance. The mass transport and charge transfer of the RCE reactor were characterized under turbulent flow by means of the dimensionless Damköhler (*Da*) number, as well as from the Sherwood-Reynolds-Schmidt (*Sh-Re-Sc*) analysis. A mixed regime with a prevalence of mass transport control was determined at E_{cath} from -1.8 V. The $Sh = 0.70Re^{0.46}Sc^{0.356}$ correlation obtained for this reactor may serve to guide the scale-up of electrochemical NO_3^- removal as more electrocatalytic cathode materials are developed. Successful NO_3^- elimination from solutions with low conductivity that mimicked groundwater is finally reported.

Keywords: Electrochemical denitrification; Electroreduction; Groundwater treatment; Hydrogen radical; Rotating cylinder electrode

1. Introduction

Nitrate removal from surface water and groundwater has attracted increasing attention in recent years, since its progressive accumulation critically endangers freshwater reservoirs worldwide [1-3]. Recent transnational reports [4] have documented that the main sources for nitrate accumulation in groundwater are the leaching of the nitrogen-based fertilizers used in intensive agriculture and the livestock manure spreading on land, whereas surface water is mostly polluted by discharge of wastewater that contains high concentration of nitrogen species. Biotic and abiotic processes cause the conversion of these species into nitrate [5], which shows great stability and solubility in water alongside poor adsorption or precipitation. The removal of this toxic ion from aqueous matrices has been investigated by several physicochemical processes like adsorption [6], biological denitrification [7], coagulation [8], chemical reduction [9] and catalytic reduction [10], as well as electrocoagulation [11,12], bioelectrochemical [13,14] and electroreduction [15,16] methods. The latter approach has led to sound results, which combines with its operational simplicity, although the mechanism involved is complex and not fully understood yet. The effect of different parameters on NO_3^- electroreduction has been studied, including the cathode material [17,18], the electrolyte concentration [19], the electrolyte composition [20-22], the pH [23] and the cell configuration (i.e., single- or double-chamber cell) [24,25].

The NO_3^- electroreduction is an electrocatalytic process that involves several species with nitrogen valence number varying from +V to -III [26]. Several mechanisms, involving either direct or indirect pathways, have been proposed for this process depending on the cathode material and the applied cathode potential (E_{cath}) [27]. In the direct pathway, which is typical for diluted nitrate solutions (< 1 M) at near-neutral or alkaline pH, adsorbed NO_3^- ions are reduced by electrons supplied to the cathode. In the mediated or indirect route, NO_3^- reacts with adsorbed atomic hydrogen (or hydrogen radical) originated as an intermediate of the hydrogen evolution reaction (HER) (1) [28]. The NO_3^- electroreduction yields the adsorbed NO_2^- from reaction (2), which can be the rate-

determining step of the process, involving 2 electrons. The subsequent NO_2^- electroreduction yields NH_3 or N_2 (6-electron steps) via reactions (3) and (4), respectively. Worth noting, some authors have reported lower energetic barriers for the indirect hydrogen radical (•H) mechanism leading to NH_3 [28].

$$2H_2O + 2e^- \rightarrow H_2 + 2OH^- \quad (1)$$

$$NO_3^- + H_2O + 2e^- \rightarrow NO_2^- + 2OH^- \quad (2)$$

$$NO_2^- + 5H_2O + 6e^- \rightarrow NH_3 + 7OH^- \quad (3)$$

$$2NO_2^- + 4H_2O + 6e^- \rightarrow N_2 + 8OH^- \quad (4)$$

The distribution of final by-products strongly depends on the selectivity of the cathode material for the NO_3^- conversion, being usually NO_2^- and NH_4^+/NH_3 the main nitrogen species accumulated in the treated solution. However, there are other parameters that can also affect the final speciation of those products, such as the nitrate and electrolyte concentration [19], the electrolyte composition, the pH, the temperature, the cell configuration and the residence time [19-25]. It has been reported that cathodes containing iron minimize the NO_2^- accumulation [17,21,29]. NH_3 can be easily removed from the solution due to its high volatility at alkaline pH or, alternatively, it can be recovered as a value-added product. This introduces a paradigm shift, turning water decontamination into a waste valorization strategy [30]. High selectivity for conversion into molecular N_2 could also be of interest, since it is non-hazardous and can be accumulated in the atmosphere, but it is not easy to demonstrate its predominance over other gaseous nitrogen products such as NH_3 or N_xO_y. Some density functional theory (DFT) calculations combined with experimental data reveal that the NH_3 generation is more kinetically favored due to lower energy barriers [28,31,32].

Figures of merit such as faradaic efficiency (FE) and energy consumption (EC) change notably depending on the reactor design [33,34]. The interplay between the applied E_{cath} and the system hydrodynamics determines the operational conditions needed to establish a charge transfer-controlled

regime, mass transport-controlled regime or mixed regimes. The hydrodynamics becomes relevant when the pollutant removal kinetics is partially or totally controlled by the supply of the electroactive species to the electrocatalytic surface and hence, increasing the mass transport coefficient at a fixed E_{cath} leads to a more efficient decontamination with lower energy consumption.

Different electrochemical reactor configurations have been used for NO_3^- electroreduction, in batch or in continuous mode. Planar electrodes have shown unexpectedly high efficiencies at low current, whereas fluidized beds of inert particles enhance the mass transport and the FE [35]. Membrane flow-through [36] and thin-layer [37] reactors have also been considered. Conversely, the rotating cylinder electrode (RCE) reactor has been mostly used for mass transport-controlled cathodic processes like metal recovery in the electroplating sector [38,39,40,41], as well for erosion and corrosion studies since they allow a turbulent flow at low Reynold's (*Re*) numbers from 100 [42]. This reactor enhances the mass transport of the electroactive species toward the cathode at a relatively low rotational speed [43,44], and its characterization has been made by correlation of dimensionless numbers that predict the mass transport rates for several electroactive species under a range of hydrodynamic conditions [45,46]. To our knowledge, only a single paper has addressed the electrochemical removal of nitrate with this type of reactor, employing an activated copper RCE and operating under periodic potential reversal to ensure the reactivation of the cathode surface, thus obtaining a high FE and selectivity for NH_3 [47]. However, the mass transport has not been specifically characterized for NO_3^- electroreduction in an RCE reactor.

The electrochemical denitrification opens a window of opportunity for NO_3^- elimination from polluted freshwater resources like groundwater below 50 mg L^{-1}, the threshold value established by the World Health Organization (WHO) [48]. Devices with high removal efficiency, ease of operation and low overall cost are under investigation [49]. In this context, the development and characterization of RCE reactors is required because they easily promote the turbulence and hence, the mass transport, eventually enhancing the efficiency of the denitrification treatment.

This work is focused on the characterization of the mass transport and charge transfer of an RCE reactor used for the overall NO_3^- electroreduction from a synthetic aqueous solution with high conductivity. Stainless steel and carbon steel have been considered as cheap cathode materials to compare their effectiveness to remove NO_3^- by linear sweep voltammetry (LSV). The effect of E_{cath} and rotational speed (ω) on the process performance has been studied. From these results, the RCE reactor has been characterized under turbulent flow regime by means of the dimensionless Damköhler (*Da*) number, as well as from the Sherwood-Reynolds-Schmidt (*Sh-Re-Sc*) correlation for NO_3^-removal. Finally, preliminary promising results to remove NO_3^- under galvanostatic conditions using solutions with low conductivity, mimicking a groundwater treatment, are reported. The novelty of the work lies in demonstrating the high electrocatalytic activity of a cheap carbon steel RCE to remove nitrate from water, also showing the positive effect of mass transport promotion. Moreover, a thorough characterization of this reactor is provided through the effectiveness factor, being possible to predict the nitrate removal rate once the charge transfer kinetics is elucidated.

2. Materials and methods

2.1. Reagents

Sodium hydroxide (> 99% purity), potassium nitrate (> 99% purity) and potassium sulfate (99.5% purity) were purchased from Fermont. Sodium sulfate (99.0% purity), sulfuric acid (analytical grade, 95-98% purity) and tri-distilled water were provided by Karal. 5,5-Dimethy-l,1-pyrroline N-oxide (DMPO) used for electron paramagnetic resonance (EPR) analysis, as well as phthalic acid (99.5% purity) and tris(hydroxymethyl)aminomethane (99.8% purity) as mobile phase reagents for ion chromatography (IC), were purchased from Sigma-Aldrich. Analytical grade sodium nitroprusside dihydrate from Merck, phenol (> 99% purity) from Sigma-Aldrich and EDTA (> 99% purity) from Karal were used for ammonium/ammonia colorimetric determination.

2.2. Electrochemical setup

The RCE reactor consisted of a rotating cylinder cathode surrounded by 6 anode plates, as shown in Fig. 1. Two rotating cylinders with dimensions of 14.00 cm height × 3.80 cm of diameter, made of AISI 1018 carbon steel or AISI 316 stainless steel (SS316), were built as working electrodes (WE). Commercial Ti|IrO_2 (DSA-O_2, NMT Electrodes) anodes were used as counter electrode (CE). The total cathode and anode areas were similar (~100 cm^2), being the exposed surface limited by polyester tape. The good stability of the electrolytic system was confirmed by the good reproducibility of data, which was ensured upon cleaning of the RCE surface before each run. To do this, the cylinder surface was submerged in 20% H_2SO_4 for 30 s, rinsed with tri-distilled water and, finally, dried with paper.

The experiments were carried out by electrolyzing 400 mL of solutions containing 10 mM $NaNO_3$ + 0.50 M Na_2SO_4 in tri-distilled water at natural pH 6.5, placed in a jacketed open glass cell with temperature fixed at 25 ºC by recirculating thermostated water. Most trials were made in potentiostatic mode at constant E_{cath}, controlled by a double junction saturated mercury-mercurous sulfate electrode (MSE) (E^o = +0.64 V vs SHE) as reference electrode (RE), using a Biologic SP-150 power supply equipped with a Biologic VMP3B-10 booster. Some specific assays in low conductivity medium were performed under galvanostatic conditions at constant current (I) with the same instruments. The potentiostatic electrolytic trials were made in a three-electrode cell to study the effect of E_{cath} between -1.6 and -2.2 V and that of rotational speed (ω) between 100 and 500 rpm, all of them with a duration of 120 min. The final pH in these assays was approximately 12.5. The galvanostatic electrolytic trials were made at current density (j) of -12 mA cm^{-2} for 120 min in a two-electrode cell, studying the effect of the Na_2SO_4 concentration between 0.01 and 0.50 M. Some blank experiments were performed to assess the extent of ammonia volatilization.

2.3. Analytical and electrochemical characterization

The solution pH was measured with a HI 3221 pH/ORP/ISE meter from Hannah Instruments. Nitrate concentration was determined by injecting 20 µL aliquots into a Perkin Elmer ion

chromatograph coupled to an Adept Cecil CE4710 conductivity detector controlled by Chromera software. A Shim-Pack IC-A1 anion column with dimensions of 100 mm × 4.6 mm (i.d.), at 25 ºC, was used. The mobile phase was a solution composed of 2.4 mM tris(hydroxymethyl)aminomethane + 2.6 mM phthalic acid (pH 4), which was eluted at 1.5 mL min^{-1}, displaying the nitrate peak at 4.6 min. The ammonia concentration was obtained by means of the standard indophenol blue colorimetric method, which required the measure of the absorbance at 645 nm using a PerkinElmer Lambda 35 UV/Vis spectrophotometer.

LSV was performed with a Biologic SP-150 potentiostat controlled by EC-LAB v11.10 software. A rotating disk electrode (RDE) made of AISI 1018 steel or SS316 with 4.5 mm diameter was used as WE. The CE was a graphite bar and the RE was the saturated $Hg|Hg_2SO_4$ electrode mentioned above. The solutions contained up to 10 mM KNO_3, with 0.50 M Na_2SO_4 as supporting electrolyte, and the voltammograms were recorded starting from the open circuit potential (E_{OCP} = -1.050 V vs MSE), at a scan rate of 5 mV s^{-1}.

The possible generation of hydrogen radical during the nitrate electrocatalytic reduction was assessed by EPR using DMPO as the spin-trapping agent. AISI 1018 steel and SS316 plates of 5 cm^2 were used as cathode, at E_{cath} = -1.80 V. A Pt plate with analogous surface area was used as counter electrode. The in-situ electrogeneration of the adsorbed •H, in the form of DMPO-H adduct, was carried out in 15-mL solutions in the presence and absence of 10 mM nitrate after addition of 16.90 µL of 10 mM DMPO, using a single-chamber cell (SCC) under continuous magnetic stirring. 2.0 mL of samples were collected and placed in plastic tubes at 0, 5 and 20 min, immediately frozen by contact with dry ice and further, thawed and introduced into a quartz tube to be analyzed, always after the same time period from initial sampling. The EPR spectra were recorded in a Bruker ESP300E spectrometer at room temperature, fixing the following parameters: resonance frequency of 9.79 GHz, microwave power of 2 mW, modulation amplitude of 1.0 G, sweep width of 100 G (3450-3550), time constant of 40.96, sweep time of 83.97, and receiver gain of 2×10^4.

2.4. Theory and calculations

The faradaic efficiency (FE) for nitrate electroreduction and the energy consumption per nitrate gram (EC) were calculated by the following expressions [50]:

$$\mathrm{FE} = \frac{nF(C_0 - C_t)V}{Q_t} = \frac{nF(C_0 - C_t)V}{It} \quad (5)$$

$$\mathrm{EC\ (Wh\ g^{-1})} = \frac{E_{cell}Q_t}{3600(C_0 - C_t)MV} = \frac{E_{cell}It}{3600(C_0 - C_t)MV} \quad (6)$$

where n is the global number of electrons transferred according to consecutive reactions (2) and (3), accounting for the complete reduction of nitrate to ammonia (n = 8), F is the Faraday constant (96,485 C mol^{-1}), C_0 is the initial nitrate concentration (0.010 M) and C_t is the nitrate concentration at given time (in M), V is the solution volume (0.4 L), M is the nitrate molar mass (62 g mol^{-1}) and Q_t is the charge at the same time (in C).

The Koutecky-Levich (K-L) equation (7) and its derived Eq. (8) were applied to analyze the linear sweep voltammograms recorded with an RDE as WE [50]:

$$\frac{1}{I_c} = \frac{1}{I_k} + \frac{1}{I_l} \quad (7)$$

$$\frac{1}{I_c} = \frac{1}{nFAk_hC^*} + \frac{1}{0.62nFAD_t^{2/3}\nu^{-1/6}\omega^{1/2}C^*} \quad (8)$$

where I_c is the measured current, I_k is its kinetic term (in the absence of mass transport), I_l is the limiting diffusion current, n is the number of electrons involved in the nitrate electroreduction, A is the electrode area, D_t is the diffusion coefficient of nitrate ion, ω is the rotational speed, ν is the kinematic viscosity and C^* is the nitrate bulk concentration (10^{-2} M). The heterogeneous charge transfer constant (k_h) can then be obtained from the independent term of the linear regression at infinite ω.

The effectiveness factor (η) for the heterogeneous electroreduction process is described by Eq. (9) [51]:

$$\eta = \frac{R}{R^*} = \frac{k_1 C}{k_1 C^*} = \frac{C}{C^*} \quad (9)$$

where R is the reaction rate involving an electroactive species at concentration C, whereas R^* is that of an ideal process considering the bulk concentration C^*. In Eq. (9), it is assumed that R is described as $dC/dt = -k_1 C$ where k_1 is the global reaction rate. This means that under steady-state conditions, the species arriving by mass transport to the electrocatalytic surface disappears according to a heterogeneous charge transfer rate constant $k_h a$ [51-53], where a is the volumetric area (here, ratio between the area A of the RCE and the solution volume V inside the reactor), thereby verifying Eqs. (10)-(12):

$$k_m a(C^* - C) = k_h a C \quad (10)$$

$$C = \frac{1}{1+\frac{k_h a}{k_m a}} C^* \quad (11)$$

$$R = \eta R^* = \eta k_h a C^* \quad (12)$$

where k_m is the mass transport coefficient (m s^{-1}). The dimensionless Damköhler number (Da), which relates the charge transfer rate (intrinsic reaction) to the convective mass transport, is then defined by Eq. (13):

$$Da = \frac{k_h a}{k_m a} \quad (13)$$

As a result, the isothermal effectiveness factor η can be expressed in terms of the Damköhler dimensionless number Da from Eq. (14) [51-54]:

$$\eta = \frac{1}{1+\frac{k_h A_v}{k_m A_v}} = \frac{1}{1+Da} \quad (14)$$

Furthermore, R can be expressed by Eq. (15), leading to Eq. (16), which relates $k_h a$, $k_m a$ and k_1.

$$R = \frac{k_h a}{1+Da} C^* = \frac{k_h a}{1+\frac{k_h a}{k_m a}} C^* = \frac{1}{\frac{1}{k_h a}+\frac{1}{k_m a}} C^* \quad (15)$$

$$k_1 = \frac{1}{\frac{1}{k_h a}+\frac{1}{k_m a}} \quad (16)$$

3. Results and discussion

3.1. Comparative electrocatalytic performance of cathode materials for nitrate removal

First, the AISI 1018 steel and SS316 cathodes were electrochemically characterized by LSV to assess their electrocatalytic activity for NO_3^- electroreduction. The voltammograms were recorded in an SCC, with one of the above materials embedded in a cylindrical PTFE case to become an RDE employed as WE; a graphite bar and $Hg|Hg_2SO_4|$sat. K_2SO_4 served as CE and RE, respectively, operating at a scan rate of 5 mV s^{-1}. The assays were made with 400 mL of solutions containing 0, 2, 5 and 10 mM NO_3^- under static conditions, followed by trials made with 400 mL of 10 mM NO_3^- solutions at ω values from 100 to 3000 rpm, always using 0.50 M Na_2SO_4 as supporting electrolyte. Under static conditions, Fig. 2a highlights a well-defined wave with half-wave potential ($E_{1/2}$) of -1.58 V vs RE when using the 1018 steel cathode, which can be attributed to the NO_3^- reduction. This was confirmed by the fact that the height of the wave raised proportionally as the NO_3^- concentration in the medium was increased, suggesting that the mechanism involves the reaction (2) as rate-determining step, followed by faster successive reduction steps. In contrast, only the background signal can be observed in Fig. 2a using the SS316 cathode, being the current related to the HER because the same profile was recorded in the absence of NO_3^-. This means that this ion cannot be efficiently electroreduced on this cathode material, probably because the process is inhibited by the passivating chromite present on its surface.

Fig. 2b depicts the progressive rise in height of the reduction wave when the rotational speed of the RDE made with 1018 steel increased from 100 to 3000 rpm, owing to the gradual enhancement of the NO_3^- mass transport towards the diffusion boundary layer adjacent to the electrocatalytic

surface. However, a clear plateau was not achieved in any case, as also reported for the same reaction on copper cathode [47]. This behavior can be ascribed to the partial overlapping of the wave of NO_3^- electroreduction with the slightly more negative background signal of HER (see Fig. 2a), causing a disturbance that makes it difficult to corroborate that the process under study is only controlled by mass transport. The data of Fig. 2b were then analyzed at each E_{cath} value to obtain the corresponding I^{-1} vs $\omega^{-1/2}$ relationships (K-L plot) [55], some of which (i.e., potentials between -1.60 and -1.80 V) are presented in Fig. 2c. Excellent linear correlations were found in the E_{cath} interval between -1.45 and -1.85 V, with decreasing slopes varying from 10115 to 867 $rad^{1/2}\ s^{-1/2}\ A^{-1}$ and $R^2 > 0.983$. This allowed the calculation of the total number of electrons n involved in the NO_3^- electroreduction. Fig. 2d shows a reverse sigmoidal profile of n vs E_{cath}, which is typical of a sluggish reaction. In this case, the n value increased gradually at higher E_{cath}, up to a value close to 8 at -1.80 V and beyond. This can be confirmed from Fig. 2c, where the linear regressions depicted at E_{cath} = -1.80 V is parallel to the theoretical trend assuming n = 8. This number of transferred electrons corresponds to the selective conversion of NO_3^- to NH_3 via the global reaction (17), which is the sum of reactions (2) and (3). This full reduction of the NO_3^- with an oxidation state of (+V) to NH_3 nitrogen (-III) can be associated to successive faster rate steps after the two-electron rate-limiting reaction (2) of the adsorbed NO_3^- to NO_2^-, occurring on the 1018 steel cathode electrocatalytic surface.

$$NO_3^- + 6H_2O + 8e^- \rightarrow NH_3 + 9OH^- \quad (17)$$

From the above K-L analysis, the k_h resulting at given E_{cath} values was determined from Eq. (8), as has been collected in Table 1. For this calculation, the diffusion coefficient of NO_3^- ($D_{(NO3^-)}$ = 1.90 $\times 10^{-5}\ cm^2\ s^{-1}$) and the kinematic viscosity of the solution (ν = 0.0088 $cm^2\ s^{-1}$) were used [35].

Fig. 3a shows the EPR spectra recorded with DMPO acting as the spin trap to detect the adsorbed $^{\bullet}H$ generated on the electrocatalytic surface of the 1018 steel cathode. The signal intensity increased with electrolysis time because of the larger production of $^{\bullet}H$, with a larger accumulation of DMPO-

•H. In the presence of NO_3^-, a lower signal intensity was found. This means that •H may certainly play an important role in the NO_3^- electroreduction, since it is generated in large amounts as an intermediate of the HER. The high surface mobility of •H favors its reaction with either adsorbed NO_3^- or partially reduced nitrogen intermediates, since atomic hydrogen is an efficient reducing agent. In contrast, DMPO-•H adduct was not detected when the SS316 cathode was used, as deduced from the overlapping spectrum with that of the blank solution before electrolysis. The EPR spectra from the trials with 1018 steel show the typical DMPO-•H pattern composed of 9 peaks, and Fig. 3b reveals an intensity ratio of 1:1:2:1:2:1:2:1:1 with measured hyperfine coupling constant values of a_N = 16.52 G and a_H = 22.58 G for the nitrogen and the 2 equivalent hydrogen atom nuclei, respectively, in agreement with those determined in the literature [56].

3.2. Potentiostatic nitrate removal using an RCE reactor

The NO_3^- removal was subsequently studied employing a 100 cm^2 1018 steel cathode as WE in an RCE. Fig. 4a depicts the effect of the E_{cath}, from -1.65 to -2.2 V, applied to the cathode for the treatment of 400 mL of solutions containing 10 mM KNO_3 + 0.50 M Na_2SO_4 at 25 ºC and ω = 300 rpm. As expected, a more negative E_{cath} accelerated the NO_3^- electroreduction and 100% removal was achieved after 100-120 min of electrolysis from E_{cath} -1.80 V. This is due to the increase of the applied overpotential, which enhances the charge transfer kinetics for the rate-limiting reaction (2), achieving the complete NO_3^- removal at E_{cath} = -1.80 V with n = 8 (see Fig. 2d), i.e., when all the ion is selectively converted into N-ammonia. Therefore, these E_{cath} values were selected as optimal for subsequent trials. The kinetic analysis of the above concentration decays revealed that they obeyed a first-order reaction, as expected if the electrode reaction (2) is the rate-determining step. The good linear plots obtained in this analysis are shown in Fig. 4b and the corresponding k_1-values with excellent fittings (R^2 > 0.996) are summarized in Table 1. The k_1-value grew 4.1 times when E_{cath}

varied between -1.65 and -2.20 V (i.e., 1.9×10^{-4} s^{-1} vs 7.7×10^{-4} s^{-1}), suggesting that the electrocatalytic activity of the cathode was maintained in all the trials.

The concentration of generated N-ammonia was measured during the trials of Fig.4a, and its normalized accumulation over the initial N-nitrate concentration (10 mM) is given in Fig. 4c. The accumulated N-ammonia increased at more negative E_{cath}, attaining similar profiles for the fastest trials (E_{cath} from -1.80 V). However, maximum accumulation values of 67-72% at 60 min of electrolysis were obtained under these conditions, very far from 100% expected for total conversion of NO_3^- into NH_3. This apparent discrepancy can be explained by the gradual volatilization of NH_3 from the solution at alkaline pH, since the pK_a of its acidic form NH_4^+ is 9.26. Note that during the electrolysis, the solution pH changed from an initial value of 6.5 to a final value of 12.5 as result of the positive global balance of OH^- ions generated for each NO_3^- molecule removed (reaction (17)). This means that, after 60 min of treatment, the solution became highly alkaline and NH_3 loss was evidenced, thus dropping its accumulation in the medium. This explains the progressive decay of accumulated N-ammonia in Fig. 4c at $E_{cath} \geq$ -1.80 V at times longer than 60 min, reaching 55% of accumulation at 120 min. To confirm the NH_3 loss during the assays, the total nitrogen (TN), i.e., the sum of soluble N-nitrate and N-ammonia, of the electrolyzed solutions was calculated. As can be seen in Fig. 4d, TN underwent a slow and gradual abatement regardless of the applied E_{cath}, losing a 37% at E_{cath} =-1.60 V and up to 45-47% at $E_{cath} \geq$ -1.80 V, i.e., when larger amount of N-ammonia was produced. This decay in TN justifies the progressive volatilization of the final NH_3 due to the solution alkalinization during electrolysis. If needed, this loss might be avoided by regulating the pH around its initial value of 6.5, although this should be explored in a focused work.

The FE and EC values during the above experiments were calculated from Eqs. (5) and (6), respectively, only considering the change in NO_3^- concentration. Fig. 4e highlights that FE dropped with rising E_{cath}, reaching decreasing values of 64%, 44%, 31%, 18% and 12% after 120 min of electrolysis at -1.65, -1.70, -1.80, 1,90 and -2.20 V, respectively. Consequently, the highest FE was

achieved at E_{cath} = -1-65 V. The opposite trend followed by EC can be observed in Fig. 4f, with increasing maximum values of 15.2, 26.5, 65.8, 79.6 and 134.8 Wh g^{-1}. This loss of performance is attributable to the smaller NO_3^- coverage on the cathode surface, which is necessary for further electroreduction, and can be explained by three main reasons: (i) the progressive loss of NO_3^- concentration as the electrolysis is prolonged, (ii) the competitive electroreduction of nitrogen by-products that are fully converted into NH_3, also causing a FE decay and EC rise at longer time, and (iii) the increase in rate of the parasitic HER, taking place in a greater number of active sites, eventually causing a drop in efficiency at higher E_{cath}.

Next study aimed at assessing the influence of ω on the NO_3^- electroreduction process. To do this, 400 mL of solutions with 10 mM KNO_3 + 0.50 M Na_2SO_4 at 25 ºC were electrolyzed at E_{cath} = -1.80 V, with ω values from 100 to 500 rpm using the 1018 steel RCE. Fig. 5a makes in evidence a greater NO_3^- removal as ω raised due to the promotion of the diffusion-convection that enhances the mass transport of the ion toward the cathode. While 98% removal was achieved after 120 min at ω = 100 rpm, overall electroreduction was obtained at the same time at ω = 300 rpm and even at shorter time of 100 min at ω = 500 rpm. This tendency can also be deduced from the excellent first-order kinetics followed by the concentration decays, as depicted in Fig. 5b. The k_1-value thus determined progressively grew from 4.5×10^{-4} s^{-1} at ω = 100 rpm to 7.8×10^{-4} s^{-1} at ω = 500 rpm. These findings are indicative of the process improvement at higher rotation.

The profiles related to the NH_3 accumulation upon change of ω are shown in Fig. 5c. A maximum accumulation close to 56-57% was always reached, regardless of the applied ω. This maximum value was attained after 40 min at 400 and 500 rpm, and at progressively longer times of 60, 80 and 100 min when ω decreased from 300 to 200 and 100 rpm, owing to the worsen diffusion-convection that led to a slower NO_3^- electroreduction, as stated above. Once the maximum NH_3 was accumulated, its volatilization predominated over its accumulation, giving rise to a gradual loss of its concentration

from 51% at ω = 100 rpm to 38% at ω = 500 rpm. The occurrence of a quicker NH_3 concentration abatement at higher ω was expected in the alkalinized medium, as typically observed for volatiles retained in aqueous media. This behavior can be confirmed from the calculated TN variations presented in Fig. 5d. While 48% of TN was reduced after 120 min at 100 and 200 rpm, higher and increasing TN decays of 51%, 56% and 62% were found at 300, 400 and 500 rpm as result of the gradual greater formation and volatilization of NH_3 due to the quicker NO_3^- electroreduction. These results agree with those pointed out above in Fig.4d.

A last series of experiments was made with 400 mL of solutions containing 5 mM $(NH_4)_2SO_4$ (i.e., 10 mM of NH_4^+) + 0.50 M Na_2SO_4 at pH 12.0, using a SS316 cylinder in a RCE reactor with rotation between 100 and 500 rpm, but without current supply. These non-electrochemical blank trials were made to confirm the NH_3 volatilization under the alkaline conditions tested. Fig. 5e reveals quite similar profiles for the loss of N-ammonia concentration to those shown in Fig. 5c. Thus, after 120 min, Fig. 5e shows that the NH_3 concentration was progressively reduced by 41%, 47%, 54%, 69% and 66% operating at 100, 200, 300, 400 and 500 rpm. These values are slightly higher than those found for the loss of N-ammonia in Fig. 5c because of the higher initial NH_3 used. Hence, these findings corroborate the occurrence of a quicker volatilization of NH_3 at higher ω, favored by a more turbulent flow ($8592 \leq Re \leq 42959$), which impedes an accurate calculation of the yield rate for converting nitrate to ammonium.

3.3. Mass transport characterization of nitrate removal

The assays described above allowed the determination of the k_1-values corresponding to the NO_3^- electroreduction process from a 10 mM NO_3^- + 0.50 M Na_2SO_4 solution using a 1018 steel RCE. The data obtained at different E_{cath} values at ω = 300 rpm are collected in Table 1, whereas those found at E_{cath} = -1.80 V and different ω values are summarized in Table 2. These results make in evidence that the system operates under diffusion-convection conditions, being insignificant the migration of NO_3^-

ions due the high concentration of supporting electrolyte. On the other hand, the k_h-values under the same conditions were determined from the aforementioned K-L analysis and hence, those corresponding to different E_{cath} values at ω = 300 rpm are listed in Table 1. Based on all these data, the k_m-values of the assays were calculated from Eq. (16) considering a volumetric area of a = 0.25 cm^{-1} (i.e., A (100 cm^2) /V (400 cm^3)). Table 2 shows the k_m-values calculated for trials at different ω values and E_{cath} = -1.80 V.

Once determined the k_h and k_m parameters for each assay, the dimensionless Damköhler number was obtained from Eq. (9), and the values obtained are given in Tables 1 and 2. This parameter is very relevant because, from the effectiveness factor η calculated by Eq. (14) that must range between 0 and 1 [52], it informs about the regime that controls the process. So, for high Da values, the effectiveness factor will tend to 1/Da and hence, to 0, meaning that the process is under mass transport control regime and $k_1 = k_m a$. In contrast, for small Da values, η will tend to 1, picturing that the process is controlled by charge transfer and $k_1 = k_h a$. In intermediate situations, the process will be under a mixed regime with no predominance of neither mass transport nor charge transfer. In the present RCE reactor, Fig. 6a and 6b show the change of η with the overpotential in absolute value ($|E_{cath} - E_{OCP}|$) and with the dimensionless Reynolds (Re) number, respectively. The latter term was calculated by Eq. (18) [52]:

$$Re = \frac{ud}{v} \tag{18}$$

where u is the peripheral velocity (= $\pi\omega d$); in this relationship, ω is expressed in rev s^{-1}, and d is the RCE diameter.

Fig. 6a shows a uniform decay of η from 0.52 to 0.20 when the absolute value of the cathodic overpotential was increased from 0.55 to 0.85 V (considering the E_{cath} data of Fig. 4 at constant ω = 300 rpm). Since the NO_3^- electroreduction process is limited by the slowest phenomenon, the trend of Fig. 6a means that the increase of the overpotential in absolute value enhanced the charge transfer

kinetics, thus making the system gradually more dependent on the mass transport. Fig. 6b highlights a rise of the effectiveness factor from 0.20 to 0.35 for *Re* varying from 8592 to 42959 (see assays of Fig. 5a at E_{cath} = -1.80 V). As the rotation of the RCE is increased, the fluid becomes more turbulent and the mass transport toward the cylindric electrode is enhanced (i.e., the Nernst diffusion layer becomes thinner), thus increasing the relevance of the charge transfer rate. Based on the intermediate values obtained for η (i.e., between 0.20 and 0.35) in the selected ranges of E_{cath} and ω, it can be concluded that the system is under mixed control regime [53]. It is worth mentioning that the effectiveness factor is an indicator of how efficient is the mass transport; i.e., if a very fast charge transfer process exists, an efficient mass transport will be required to have $k_h a = k_m a$, and therefore, $Da \rightarrow 1$ with $\eta \rightarrow 0.5$. The RCE is suitable to achieve such condition because of the resulting turbulence; just for comparison, the η values would tend to zero in a parallel plate electrochemical reactor because the inertia of the fluid does not generate the high turbulence promoted in an RCE. From the data obtained here, the electrochemical NO_3^- reduction on the electrocatalytic 1018 steel (at E_{cath} = -1.80 V) occurs under excellent mass transport. NO_3^- electroreduction is thus substantially dependent on the charge transfer kinetics although, under certain experimental conditions, it is revealed to be shifted toward a larger mass transport control.

Eq. (16) makes it possible to treat the mass transport coefficient separately, by obtaining an additional correlation that describes its dependence on the hydrodynamics imposed by the RCE. The reactor characterization described in previous subsections allowed determining the dimensionless Sherwood (*Sh*) and Schmidt (*Sc*) values as follows [46]:

$$Sh = \frac{k_m d}{D} \tag{19}$$

$$Sc = \frac{\nu}{D} \tag{20}$$

The *Sh* number correlates convective mass transport with pure diffusion, whereas the *Sc* number correlates momentum diffusivity with molecular diffusion. The *Sh*-values obtained from the trials of Fig. 5 are collected in Table 2. These parameters accomplish the following correlation [46]:

$$Sh = \alpha Re^{\beta} Sc^{\gamma} \quad (21)$$

where α is a coefficient related to the reactor dimensions, shape of the electrode and electrolyte properties, β is associated with the hydrodynamic regime, and γ = 0.356 is characteristic of the RCE reactor configuration [42-43,46]. Fig. 7 shows the good linear ln (Sh /$Sc^{0.356}$) vs ln *Re* plot obtained from the assays of Fig. 5, yielding values of α = 0.70 and β = 0.46 for our system, with an interelectrode gap of 2.1 cm. Rivera et al. [46] reported quite similar values of α = 0.89 and β = 0.43 using an interelectrode gap of 2.4 cm to study the I_3^-/I^- process with an SS304 RCE. In contrast, Arredondo et al. [39] obtained very different values of α = 0.11 and β = 0.99 using an SS316 RCE for Ag deposition, suggesting that the values are strongly dependent on the nature of the reduced electroactive species. Based on these evidences, it is evident that the mass transport correlations must be experimentally obtained for each particular electrochemical system.

3.4. Preliminary assessment of the RCE reactor for groundwater treatment

A crucial conclusion from results reported in previous sections is that, knowing the *Sh-Re-Sc* correlation and the k_h values for NO_3^- electroreduction on a given cathode, the removal rates of this ion would be fully predictable for treating actual wastewater with sufficient conductivity that enables the operation under convection-diffusion conditions. This is feasible, for example, when NO_3^--polluted effluents are pre-treated with ion exchange resins, further generating rinsing solutions highly concentrated with desorbed NO_3^-. In such cases, the electroreduction process in a scaled-up RCE reactor would be fully controlled. To assess the possibility of treating NO_3^- in less conductive media (e.g., groundwater) than that studied so far, model solutions with lower concentrations of supporting

electrolyte were prepared. Electrolytic trials were performed in galvanostatic mode because of its greater simplicity, envisaging a future application.

The effect of the supporting electrolyte concentration (10-500 mM Na_2SO_4) over the electroreduction of 400 mL of 10 mM NO_3^- solutions was then studied in the same RCE system described above but applying a current of -1.2 A (j = -12 mA cm^{-2}) at ω = 300 rpm (Re = 25775). At such j, the potential was -1.8 < E_{cath} < -1.6 V to favor the nitrate reduction minimizing the HER. Fig. 8a shows that NO_3^- was more rapidly removed as the Na_2SO_4 concentration was risen, i.e., at higher conductivity that enhances the diffusion-convection regime and mass transport. After 120 min of electrolysis, 94%, 95% and 97% reduction of NO_3^- was achieved at 10, 100 and 500 mM Na_2SO_4, respectively. The kinetic analysis of Fig 8b corroborates that NO_3^- decay obeyed a first-order kinetics, yielding rising k_1-values of 3.5×10^{-2}, 4.0×10^{-2} and 5.4×10^{-2} s^{-1} with excellent fittings (R^2 > 0.99). The FE values presented in Fig. 8c highlight a higher efficiency with increasing the supporting electrolyte concentration, pre-eminently at the beginning of the process when the migration is more relevant, mitigating this detrimental phenomenon as the supporting electrolyte concentration is risen. For the most efficient system (0.50 M Na_2SO_4) the FE drops from 88% to a final value of 34%, owing to the loss of NO_3^- content and the increase of the parallel reduction of water (i.e., HER) and nitrogen by-products formed. Also, the migration term becomes less important and at 120 min, the FE value is 34% regardless of the Na_2SO_4 concentration. Fig. 8d depicts a high EC decrease from 98.2 to 46.9 and 35.8 Wh g^{-1} as the Na_2SO_4 concentration increases from 10 to 100 and 500 mM, mainly due to the decay of cell voltage from 9.0 to 4.6 and 3.6 V due to the progressive rise of conductivity.

These results are promising and open the door to the application of a 1018 steel cathode in an RCE reactor for NO_3^- electroreduction in groundwater and wastewater with low conductivity. Nevertheless, strategies to increase the conductivity of the solution to be treated are welcome, since it favors the mass transport to the cathode surface by diffusion-convection, as the natural NO_3^- migration toward the anode is detrimental for its efficient abatement.

4. Conclusions

It has been shown that conductive solutions with 10 mM NO_3^- + 0.50 M Na_2SO_4 can be efficiently treated using a 1018 steel RCE under potentiostatic conditions, achieving the complete and selective conversion of NO_3^- into NH_3 via an 8-electron global reaction that involves $^{\bullet}H$ as mediator. Conversely, the process is inhibited when an SS316 cathode is used. The NO_3^- decay always obeyed a first-order reaction kinetics, in agreement with an initial two-electron reduction of NO_3^- to NO_2^- as the rate-determining step, allowing the determination of the k_1-values. Due to the spontaneous solution alkalinization, NH_3 is partially released to the atmosphere. FE values near 56% were obtained at the beginning of the process, whereas the increase of cathodic overpotential and ω accelerated the electroreduction process. From the LSV analysis and bulk electrolysis, the k_h and k_m values were determined, respectively. The diffusion-charge transfer of the RCE reactor was characterized upon calculation of the *Da* and η values, showing that it operates under a mixed regime. Key dimensionless parameters like *Re*, *Sh* and *Sc* have also been calculated, yielding a useful mass transport correlation (under turbulent flow, $8592 \leq Re \leq 42959$) for the scale-up of the process in the absence of migration. Finally, promising preliminary results have been obtained for the NO_3^- electroreduction in solutions with low conductivity using the same RCE system, thus paving the way for future studies with actual wastewater or groundwater.

Acknowledgements

The authors gratefully acknowledge financial support from projects PID2019-109291RB-I00 (MCIN/AEI/10.13039/501100011033, Spain) and CIIC 203/2022 (University of Guanajuato, Mexico), as well as the FPI PhD scholarship awarded to R.O. (BES-2017-080095, MINECO, Spain).

References

[1] D. Han, M.J. Currell, G. Cao, Deep challenges for China's war on water pollution. environmental pollution, Environ. Pollut. 218 (2016) 1222-1233. https://doi.org/10.1016/j.envpol.2016.08.078

[2] European Comission, The nitrate directive, 2021, https://ec.europa.eu/environment/water/water-nitrates/index_en.html

[3] EPA, Estimated nitrate concentrations in groundwater used for drinking, 2017. https://www.epa.gov/nutrient-policy-data/estimated-nitrate-concentrations-groundwater-used-drinking

[4] Euronews, How nitrate water pollution is posing a threat to people and ecosystems in Spain. 2022. https://www.euronews.com/2022/02/25/save-our-water-the-devastating-impact-of-nitrate-pollution-in-spain (accessed on 2 August 2022)

[5] E.E. Stüeken, M.A. Kipp, M.C. Koehler, R. Buick, The evolution of Earth's biogeochemical nitrogen cycle. Earth Sci. Rev. 160 (2016) 220–239. https://doi.org/10.1016/j.earscirev.2016.07.007

[6] H. Zhou, Y. Tan, W. Gao, Y. Zhang, Y. Yang, Selective nitrate removal from aqueous solutions by a hydrotalcite-like absorbent FeMgMn-LDH, Sci. Rep. 10 (2020) 16126. https://doi.org/10.1038/s41598-020-72845-3

[7] A. Kapoor, T. Viraraghavan, Nitrate removal from drinking water—Review, J. Environ. Eng. 123 (1997) 371-380. https://doi.org/ 10.1061/(ASCE)0733-9372(1997)123:4(371)

[8] A.A. Aghapour, S. Nemati, A. Mohammadi, H. Nourmoradi, S. Karimzadeh, Nitrate removal from water using alum and ferric chloride: a comparative study of alum and ferric chloride efficiency, Environ. Eng. Manage. J. 3 (2016) 69-73. https://doi.org/10.15171/ehemj.2016.03

[9] C. Huang, H. Wang, P. Chiu, Nitrate reduction by metallic iron, Water Res. 32 (1998) 2257-2264. https://doi.org/10.1016/S0043-1354(97)00464-8

[10] X. Huo, D. J. Van Hoomissen, J. Liu, S. Vyas, T.J. Strathmann, Hydrogenation of aqueous nitrate and nitrite with ruthenium catalysts, Appl. Catal. B: Environ. 211 (2017) 188–198. https://doi.org/10.1016/j.apcatb.2017.04.045

[11] E. Lacasa, P. Cañizares, C. Sáez, F.J. Fernández, M.A. Rodrigo, Removal of nitrates from groundwater by electrocoagulation, Chem. Eng. J. 171 (2011) 1012-1017. https://doi.org/10.1016/j.cej.2011.04.053

[12] M. Guo, L. Feng, Y. Liu, L. Zhang, Electrochemical simultaneous denitrification and removal of phosphorus from the effluent of a municipal wastewater treatment plant using cheap metal electrodes, Environ. Sci.: Water Res. Technol. 6 (2020) 1095. https://doi.org/10.1039/D0EW00049C

[13] S. Ghafari, M. Hasan, M.K. Aroua, Bio-electrochemical denitrification - a review, Bioresour. Technol. 99 (2008) 3965-3974. https://www.researchgate.net/publication/285876442

[14] G. Puiggioni, S. Milia, E. Dessi, V. Unali, N. Pous, M.D. Balanguer, S. Puig, A. Carucci, Combining electro-bioremediation of nitrate in saline groundwater with concomitant chlorine production, Water Res. 206 (2021) 117736. https://doi.org/10.1016/j.watres.2021.117736

[15] V. Rosca, M. Duca, M.T. De Groot, M.T.M. Koper, Nitrogen cycle electrocatalysis, Chem. Rev. 109 (2009) 2209-2244. https://doi.org/10.1021/cr8003696

[16] J. Gao, N. Shi, Y. Li, B. Jiang, T. Marhaba, W. Zhang, Electrocatalytic upcycling of nitrate wastewater into an ammonia fertilizer via an electrified membrane, Environ. Sci. Technol. (2022) https://doi.org/10.1021/acs.est.1c08442

[17] R. Oriol, M.P. Bernícola, E. Brillas, P.L. Cabot, I. Sirés, Paired electro-oxidation of insecticide imidacloprid and electrodenitrification in simulated and real water matrices, Electrochim. Acta 317 (2019) 753–765. https://doi.org/10.1016/j.electacta.2019.05.002

[18] A.S. Fajardo, P. Westerhoff, C.M. Sanchez-Sanchez, S. Garcia-Segura, Earth-abundant elements a sustainable solution for electrocatalytic reduction of nitrate, Appl. Catal. B: Environ. 281 (2021) 119465. https://doi.org/10.1016/j.apcatb.2020.119465

[19] I. Katsounaros, G. Kyriacou, Influence of nitrate concentration on its electrochemical reduction on tin cathode: Identification of reaction intermediates, Electrochim. Acta 53 (2008) 5477-5484. https://doi.org/10.1016/j.electacta.2008.03.018

[20] I. Katsounaros, G. Kyriacou, Influence of the concentration and the nature of the supporting electrolyte on the electrochemical reduction of nitrate on tin cathode, Electrochim. Acta 52 (2007) 6412-6420. https://doi.org/10.1016/j.electacta.2007.04.050

[21] W. Huang, M. Li, B. Zhang, C. Feng, X. Lei, B. Xu, Influence of operating conditions on electrochemical reduction of nitrate in groundwater, Water Environ. Res. 85 (2013) 224-231. https://doi.org/10.2175/106143012x13418552642047.

[22] R. Oriol, E. Brillas, P.L. Cabot, J.L. Cortina, I. Sirés, Paired electrochemical removal of nitrate and terbuthylazine pesticide from groundwater using mesh electrodes, Electrochim. Acta 383 (2021) 138354. https://doi.org/10.1016/j.electacta.2021.138354

[23] M. Dortsiou, I. Katsounaros, C. Polatides, G. Kyriacou, Influence of the electrode and the pH on the rate and the product distribution of the electrochemical removal of nitrate, Environ. Technol. 34 (2013) 373-381. 10.1080/09593330.2012.696722

[24] J. Ding, W. Li, Q.L. Zhao, K. Wang, Z. Zheng, Y.Z. Gao, Electroreduction of nitrate in water: role of cathode and cell configuration, Chem. Eng. J. 271 (2015) 252-259. http://dx.doi.org/10.1016/j.cej.2015.03.001

[25] W. Li, C. Xiao, Y. Zhao, Q. Zhao, R. Fan, J. Xue, Electrochemical reduction of high-concentrated nitrate using Ti/TiO_2 nanotube array anode and Fe cathode in dual-chamber cell, Catal. Lett. 146 (2016) 2585-2595. https://doi.org/10.1007/s10562-016-1894-3

[26] D. Xu, Y. Li, L. Yin, Y. Ji, J. Niu, Y. Yu, Electrochemical removal of nitrate in industrial wastewater, Front. Environ. Sci. Eng. 12 (2018) 9. https://doi.org/10.1007/s11783-018-1033-z

[27] Y. Wang, C. Wang, M. Li, Y. Yu, B. Zhang, Nitrate electroreduction: mechanism insight, *in situ* characterization, performance evaluation, and challenges, Chem. Soc. Rev. 50 (2021) 6720. https://doi.org/10.1039/D1CS00116G

[28] J. Li, G. Zhan, J. Yang, F. Quan, C. Mao, Y. Liu, B. Wang, F. Lei, L. Li, A. W. M. Chan, L. Xu, Y. Shi, Y. Du, W. Hao, P. K. Wong, J. Wang, S. Dou, L. Zhang, J. C. Yu, Efficient ammonia electrosynthesis from nitrate on strained ruthenium nanoclusters, J. Am. Chem. Soc. 142 (2020) 7036–7056. https://doi.org/10.1021/jacs.0c00418

[29] B.P. Dash, S. Chaudhari, Electrochemical denitrificaton of simulated ground water, Water Res. 39 (2005) 4065-4072. https://doi.org/10.1016/j.watres.2005.07.032

[30] P.H. van Langevelde, I. Katsounaros, M.T.M. Koper, Electrocatalytic nitrate reduction for sustainable ammonia production, Joule 5 (2021) 290-294. https://doi.org/10.1016/j.joule.2020.12.025

[31] J. Gao, B. Jiang, C. Ni, Y. Qi, X. Bi, Enhanced reduction of nitrate by noble metal-free electrocatalysis on P doped three-dimensional Co_3O_4 cathode: mechanism exploration from both experimental and DFT studies, Chem. Eng. J. 382 (2020) 123034. https://doi.org/10.1016/j.cej.2019.123034

[32] Y. Wang, W. Zhou, R. Jia, Y. Yu, B. Zhang, Unveiling the activity origin of a copper-based electrocatalyst for selective nitrate reduction to ammonia, Angew. Chem. Int. Ed. 59 (2020) 5350–5354. https://doi.org/10.1002/anie.201915992

[33] C.A. Martínez-Huitle, M.A. Rodrigo, I. Sirés, O. Scialdone, Single and coupled electrochemical processes and reactors for the abatement of organic water pollutants: a critical review, Chem. Rev. (2015) 13362-13407. https://doi.org/10.1021/acs.chemrev.5b00361

[34] C.A. Martínez-Huitle, M.A. Rodrigo, O. Scialdone, Electrochemical Water and Wastewater Treatment, Elsevier, First ed., Oxford, UK, 2018.

[35] M. Paidar, K. Bouzek, H. Bergmann, Influence of cell construction on the electrochemical reduction of nitrate, Chem. Eng. J. 85 (2002) 99-109. https://doi.org/10.1016/S1385-8947(01)00158-9

[36] P. Gayen, J. Spataro, S. Avasarala, A.M. Ali, J.M. Cerrato, B P. Chaplin, Electrocatalytic reduction of nitrate using Magnéli phase TiO_2 reactive electrochemical membranes doped with Pd-based catalysts, Environ. Sci. Technol. 52 (2018) 9370-9379. https://doi.org/10.1021/acs.est.8b03038

[37] M.A. Hasnat, S. Ben Aoun, M.M. Rahman, A.M. Asiri, N. Mohammed, Lean Cu–immobilized Pt and Pd films/–H^+ conducting membrane assemblies: relative electrocatalytic nitrate reduction activities, J. Ind. Eng. Chem. 28 (2015) 131-137. 1 https://doi.org/0.1016/j.jiec.2015.02.008

[38] F.F. Rivera, J. González, J.L. Nava, Copper removal from an effluent generated by a plastics chromium- plating industry using a rotating cylinder electrode (RCE) reactor, Environ. Technol. 29 (2008) 817–825. https://doi.org/10.1080/09593330801987327

[39] J.L. Arredondo, F.F. Rivera, J.L. Nava, Silver recovery from an effluent generated by plating industry using a rotating cylinder electrode (RCE), Electrochim. Acta 147 (2014) 337-342. https://doi.org/10.1016/j.electacta.2014.09.127

[40] J.E. Terrazas-Rodriguez, S. Gutierrez-Granados, M.A. Alatorre-Ordaz, C. Ponce de Leon, F.C. Walsh, The use of a rotating cylinder electrode to selective recover palladium from acid solutions used to manufacture automotive catalytic converters, J. Appl. Electrochem. 41 (2011) 89–97. https://doi.org/10.1016/10.1007/s10800-010-0212-9

[41] M. Rosales, J.L. Nava, Simulations of turbulent flow, mass transport, and tertiary current distribution on the cathode of a rotating cylinder electrode reactor in continuous operation mode

during silver deposition, J. Electrochem. Soc. 164 (2017) E3345-E3353. https://doi.org/10.1149/2.0351711jes]

[42] F.C. Walsh, G. Kear, A.H. Nahlé, J.A. Warton, L.F. Arenas, The rotating cylinder electrode for studies of corrosion engineering and protection of metals - An illustrated review, Corr. Sci. 123 (2017) 1-20. https://doi.org/10.1016/j.corsci.2017.03.024

[43] D.R. Gabe, G.D. Wilcox, J. Gonzalez-Garcia, F.C. Walsh, The rotating cylinder electrode: its continued development and application, J. Appl. Electrochem. 28 (1998) 759-780. https://doi.org/10.1023/A:1003464415930

[44] C.T.J. Low, C. Ponce de León, F.C. Walsh, The rotating cylinder electrode (RCE) and its application to the electrodeposition of metals, Aust. J. Chem. 58 (2005) 246–262. https://doi.org/ 10.1149/2.0351711jes

[45] M. Eisenberg, C.W. Tobias, C.R. Wilke, Ionic mass transfer and concentration polarization at rotating electrode. J. Electrochem. Soc. 101 (1954) 306-320. 10.1149/1.2781252

[46] F.F. Rivera, J.L. Nava, M.T. Oropeza, A. Recéndiz, G. Carreño, Mass transport studies at rotating cylinder electrode: Influence of the inter-electrode gap, Electrochim. Acta 55 (2010) 3275-3278. https://doi.org/10.1016/j.electacta.2009.12.060

[47] O. González Pérez, J.M. Bisang, Removal of nitrate using an activated rotating cylinder electrode, Electrochim. Acta 194 (2016) 448-453. https://doi.org/10.1016/j.electacta.2016.02.114

[48] World Health Organization, Guidelines for drinking-water quality, Fourth ed.. 2017.

[49] R. Oriol, D. Clematis, E. Brillas, J.L. Cortina, M. Panizza, I. Sirés, 2019, Groundwater treatment using a solid polymer electrolyte cell with mesh electrodes. ChemElectroChem, 6 (2019) 1235-1243. https://doi.org/10.1002/celc.201801906

[50] A.J. Bard, L.R. Faulkner, Electrochemical Methods, John Wiley & Sons, Second ed., New York, USA, 2001. http://dx.doi.org/10.1016/B978-0-12-381373-2.00056-9.

[51] G. Cassiere, J.J. Carberry, The interphase catalytic effectiveness factor: activity, yield and non-isothermality. Chem. Eng. Educ. 1 (1973) 22-26.

[52] J.L. Nava, E. Sosa, C. Ponce de León, M.T. Oropeza, Effectiveness factors in an electrochemical reactor with rotating cylinder electrode for the acid-cupric/copper cathode interface process, Chem. Eng. Sci. 2 56 (2001) 2695-2702. https://doi.org/10.1016/S0009-2509(00)00514-5

[53] J.L. Nava, E. Sosa, G. Carreño, C. Ponce-de-León, M.T. Oropeza, Modelling of the concentration–time relationship based on global diffusion-charge transfer parameters in a flow-by reactor with a 3D electrode, Electrochim. Acta 51 (2006) 4210-4217. https://doi.org/10.1016/j.electacta.2005.12.002

[54] J.J. Carberry, Chemical and Catalytic Reaction Engineering. Mc Graw Hill. New York, USA, 1976.

[55] S. Bae, K.L. Stewart, A. Gewirth, Nitrate adsorption and reduction on Cu(100) in acidic solution, J. Am. Chem. Soc. 129 (2007) 10171-10180. https://doi.org/10.1021/ja071330n

[56] H. Uchiyama, Q. Zhao, M.A. Hassan, G. Andocs, N. Nojima, K. Takeda, K. Ishikawa, M. Hori, T. Kondo, EPR-spin trapping and flow cytometric studies of free radicals generated using cold atmospheric argon plasma and X-ray irradiation in aqueous solutions and intracellular milieu, PLoS One 10 (2015) e0136956. https://doi.org/10.1371/journal.pone.0136956

Figure captions

Fig. 1. Sketch of the rotating cylinder electrode (RCE) reactor setup. (a) Rotating cylinder cathode and static planar anode, (b) anodic module consisting of six equidistant anodes fixed to a plastic holder, (c) zenithal view and (d) isometric view.

Fig. 2. Linear sweep voltammograms of nitrate reduction obtained using 400 mL of nitrate solutions in 0.50 M Na_2SO_4 at 25 ºC, with a 0.181 cm^2 AISI 1018 steel or SS316 RDE as WE, recorded from -1.1 to -1.9 V at a scan rate of 5 mV s^{-1}. A graphite bar was used as CE and $Hg|Hg_2SO_4|$sat. K_2SO_4 (E^o = +0.64 V vs SHE) as RE. (a) Effect of the nitrate concentration under static conditions. (b) Effect of the RDE rotational speed (ω) from 100 to 3000 rpm using a 1018 steel cathode in a 10 mM KNO_3 solution, (c) the corresponding Koutecky-Levich (K-L) plots at different E_{cath} values, and (d) number total of electrons involved in nitrate electroreduction obtained from the slope of the linear K-L regressions.

Fig. 3. (a) EPR spectra of the DMPO-H adduct generated during the galvanostatic electrolysis of solutions of 15 mL containing 10 mM DMPO + 0.050 M Na_2SO_4 using a single-chamber cell with a 5 cm^2 AISI 1018 steel or SS316 cathode and a 5 cm^2 Pt foil anode, at E_{cath} = -1.80 V vs $Hg|Hg_2SO_4|$sat. K_2SO_4 for 20 min. (b) Interpretation of a DMPO-H spectrum

Fig. 4. Influence of E_{cath}, from -1.65 to -2.2 V, on the (a) normalized nitrate concentration decay, (b) first-order kinetics for nitrate removal, (c) normalized N-ammonia accumulation, (d) normalized TN content, (e) faradaic efficiency and (f) energy consumption per gram of nitrate ion. These trials involved the potentiostatic electrolysis of 400 mL solutions of 10 mM KNO_3 + 0.50 M Na_2SO_4 at 25 ºC, using a 100 cm^2 AISI 1018 steel RCE as WE at ω = 300 rpm for 120 min. Commercial $Ti|IrO_2$ anodes of analogous total surface were employed as CE, and $Hg|Hg_2SO_4|$sat. K_2SO_4 as RE.

Fig. 5. Effect of the ω value, from 100 to 500 rpm, of the RCE on the (a) normalized nitrate concentration decay, (b) resulting first-order kinetics, (c) normalized N-ammonia accumulation and (d) normalized TN content under the same conditions described in Fig. 4, at E_{cath} = -1.8 V for 120 min. (e) Influence of ω on the time course of ammonia concentration during the electrolysis of a 5 mM $(NH_4)_2SO_4$ + 0.50 M Na_2SO_4 solution at pH 12.0, using the same RCE reactor but with the SS316 cylinder.

Fig. 6. Representation of the effectiveness factor (η) versus (a) the overpotentials (in absolute value) studied in the assays of Fig. 4, and (b) the Reynolds dimensionless number corresponding to the assays of Fig. 5.

Fig. 7. Mass transport correlation for nitrate electroreduction evaluated from the trials of Fig. 5b, using Eq. (16).

Fig. 8. Effect of the supporting electrolyte concentration on the evolution of (a) the normalized nitrate concentration decay and (b) the resulting first-order kinetics, (c) faradaic efficiency and (d) energy consumption per gram of nitrate ion. Galvanostatic trials were made with 400 mL solutions containing 10 mM KNO_3 + 10, 100 or 500 mM Na_2SO_4, using a 1018 steel RCE as the WE at ω = 300 rpm and j = -12 mA cm^{-2} for 120 min.

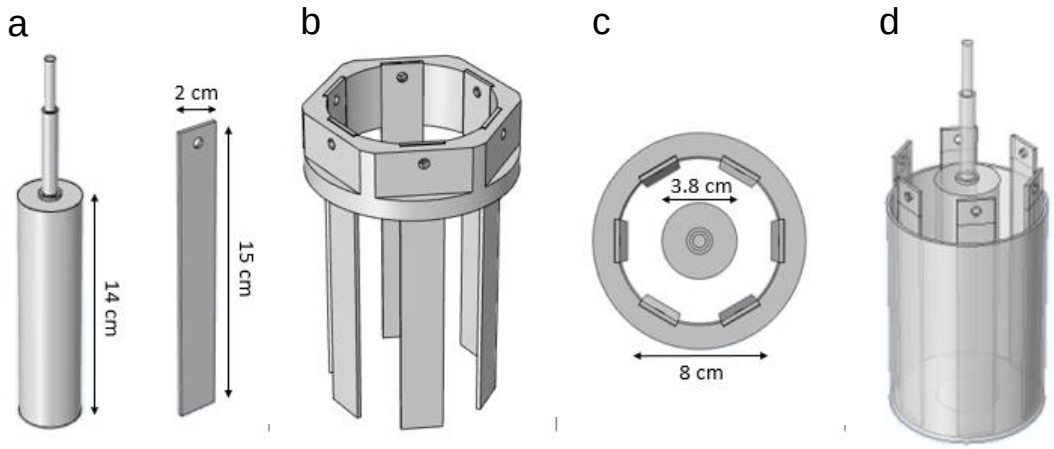

Fig. 1

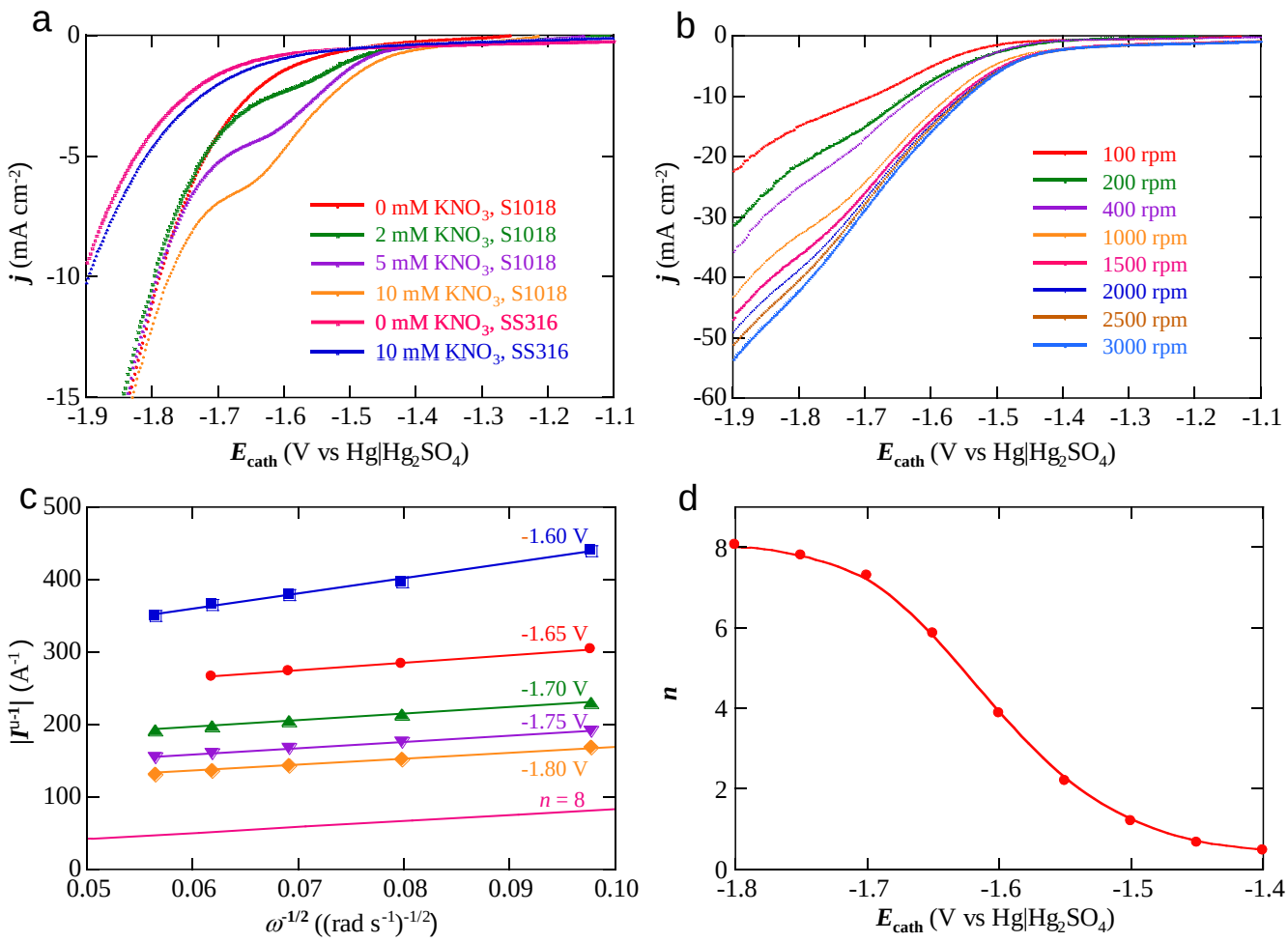
a
b
c
d
j (mA cm-2)
E cath (V vs Hg|Hg2SO4)
0 mM KNO3, S1018
2 mM KNO3, S1018
5 mM KNO3, S1018
10 mM KNO3, S1018
0 mM KNO3, SS316
10 mM KNO3, SS316
100 rpm
200 rpm
400 rpm
1000 rpm
1500 rpm
2000 rpm
2500 rpm
3000 rpm
|I u-1| (A-1)
ω-1/2 ((rad s-1)-1/2)
-1.60 V
-1.65 V
-1.70 V
-1.75 V
-1.80 V
n = 8
n

Fig. 2

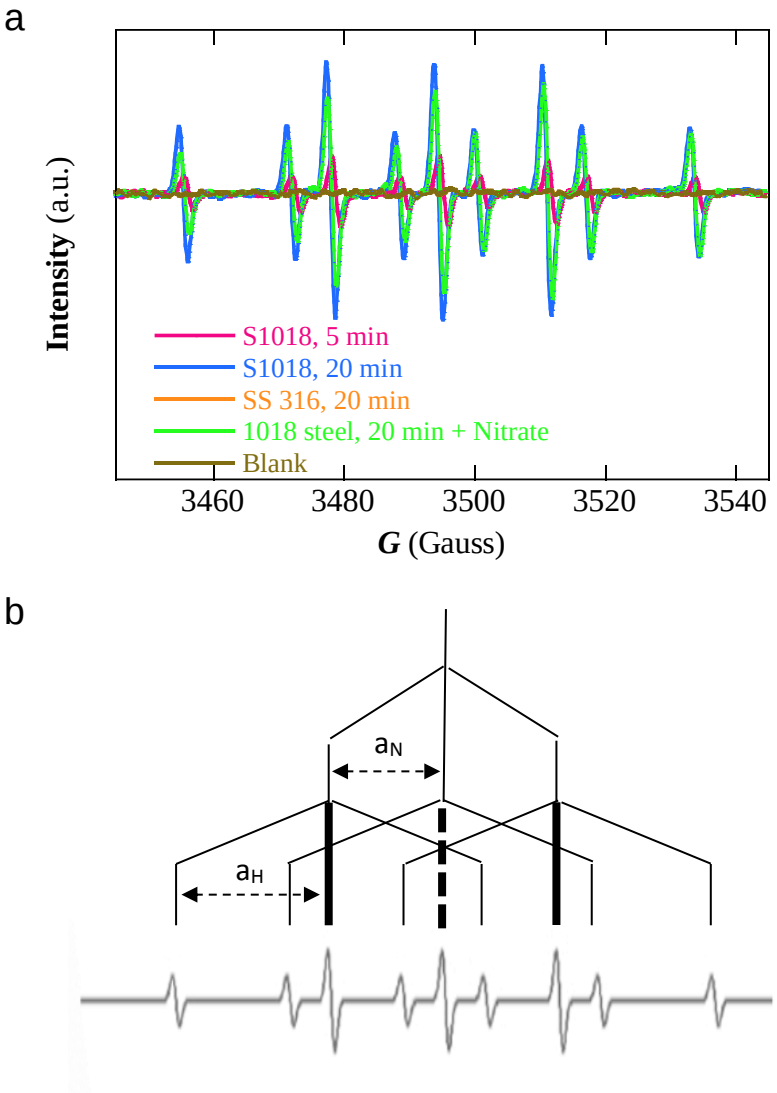
a
Intensity (a.u.)
S1018, 5 min
S1018, 20 min
SS 316, 20 min
1018 steel, 20 min + Nitrate
Blank
3460
3480
3500
3520
3540
G (Gauss)
b
aN
aH

Fig. 3

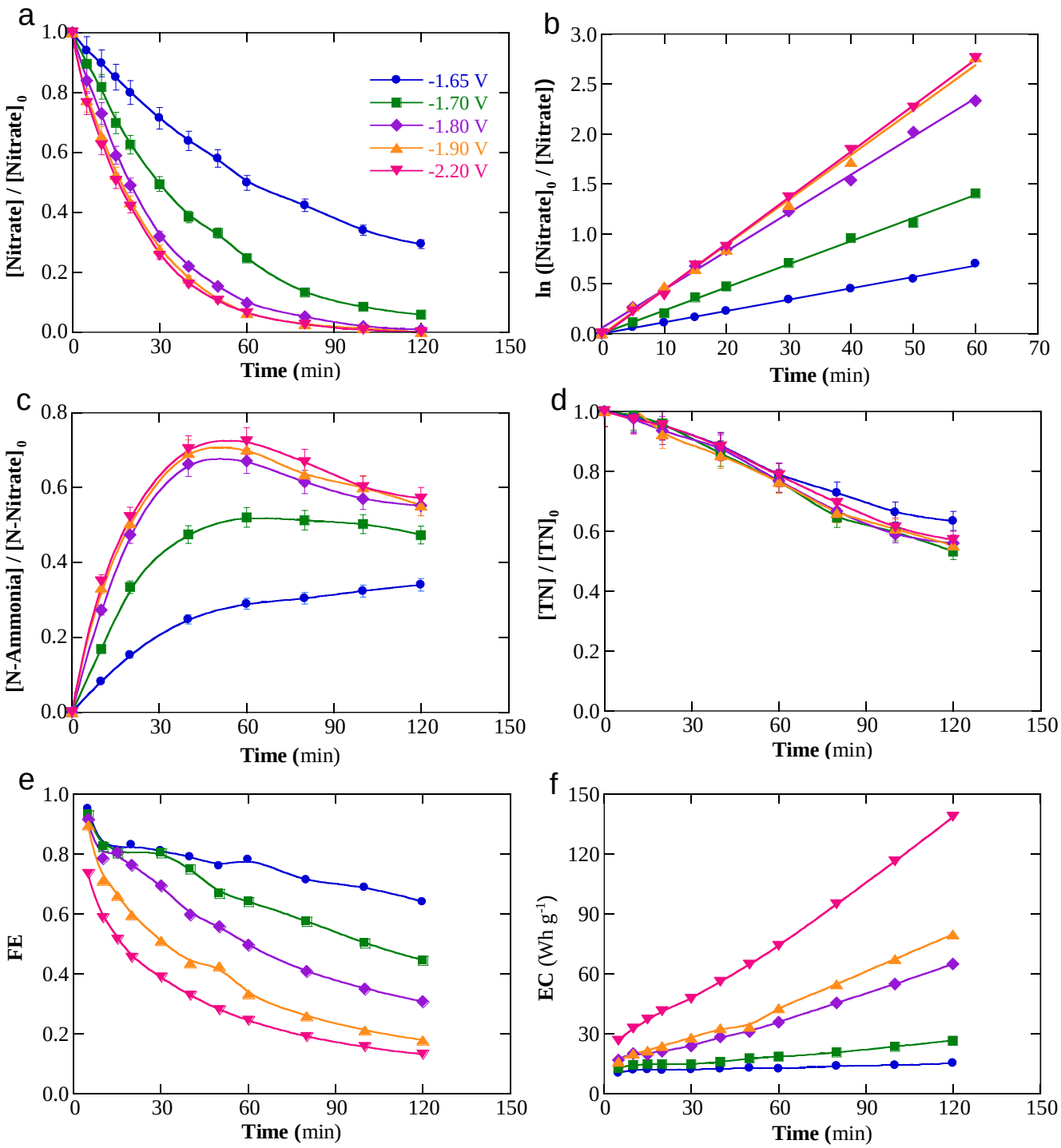
a
[Nitrate] / [Nitrate]$_0$
Time (min)
-1.65 V
-1.70 V
-1.80 V
-1.90 V
-2.20 V
b
ln ([Nitrate]$_0$ / [Nitrate])
Time (min)
c
[N-Ammonia] / [N-Nitrate]$_0$
Time (min)
d
[TN] / [TN]$_0$
Time (min)
e
FE
Time (min)
f
EC (Wh g^{-1})
Time (min)

Fig. 4

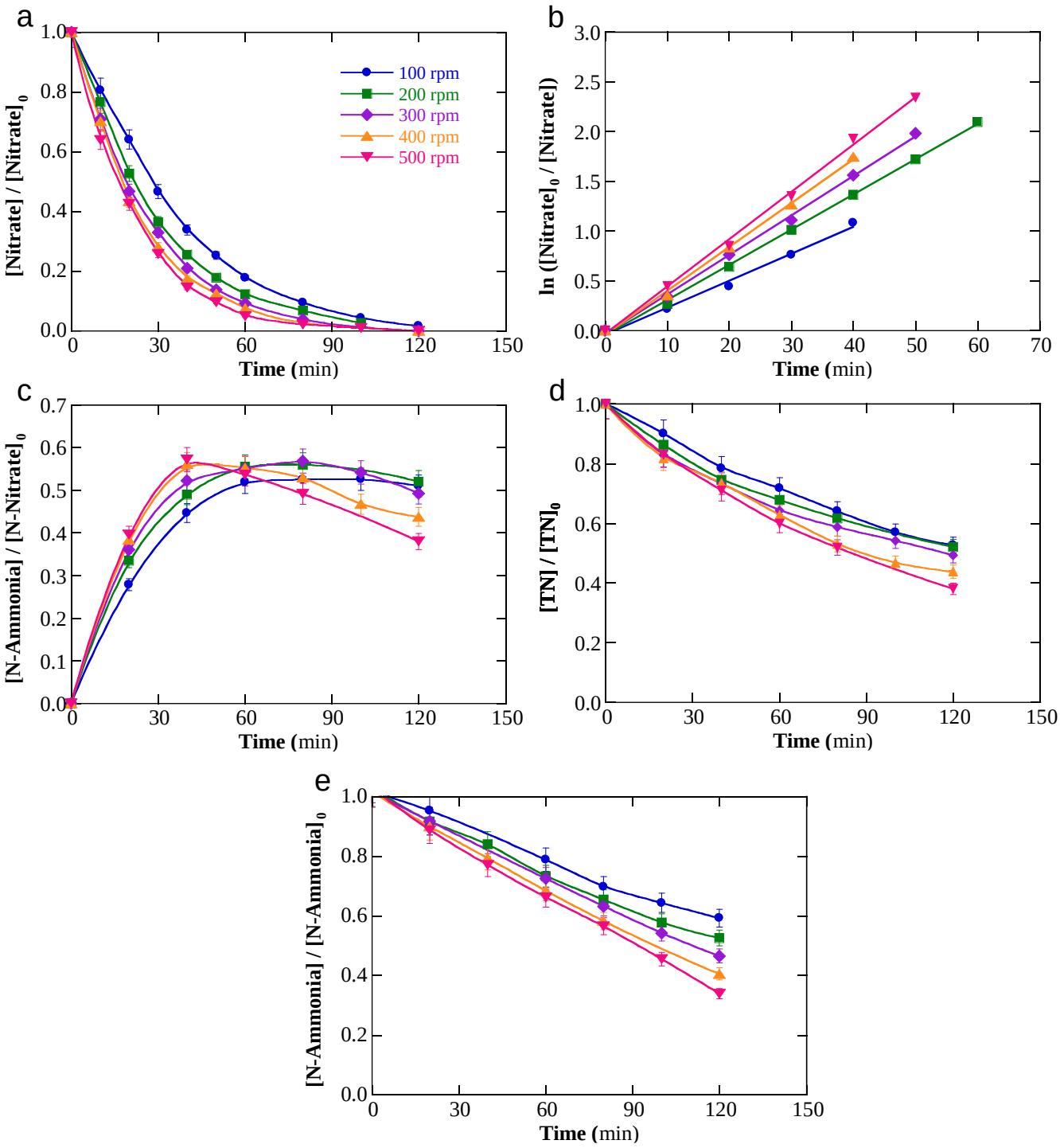
a
[Nitrate] / [Nitrate]0
Time (min)
100 rpm
200 rpm
300 rpm
400 rpm
500 rpm
b
ln ([Nitrate]0 / [Nitrate])
Time (min)
c
[N-Ammonia] / [N-Nitrate]0
Time (min)
d
[TN] / [TN]0
Time (min)
e
[N-Ammonia] / [N-Ammonia]0
Time (min)

Fig. 5

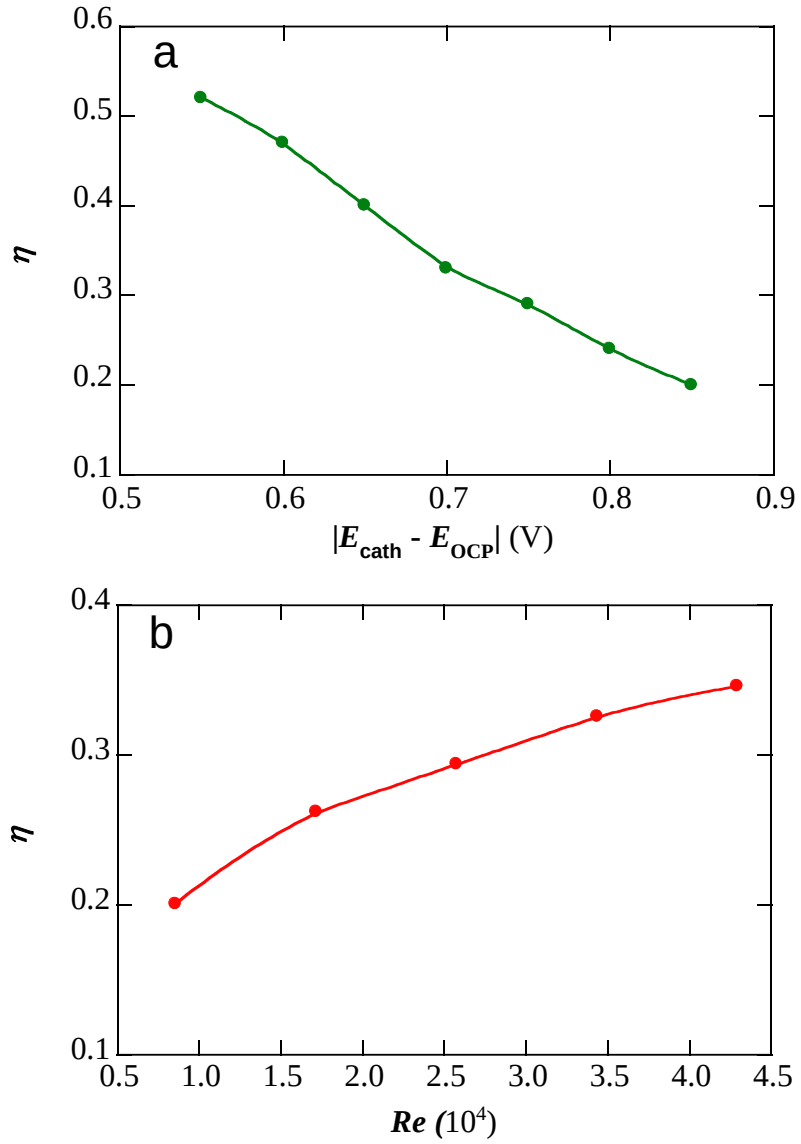
a
0.6
0.5
0.4
0.3
0.2
0.1
η
0.5
0.6
0.7
0.8
0.9
|E_cath - E_OCP| (V)
b
0.4
0.3
0.2
0.1
η
0.5
1.0
1.5
2.0
2.5
3.0
3.5
4.0
4.5
Re (10^4)

Fig. 6

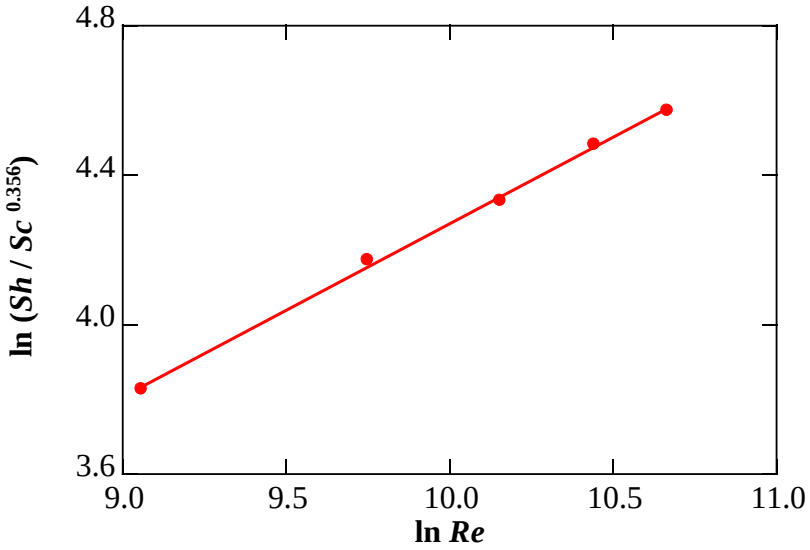

Fig. 7

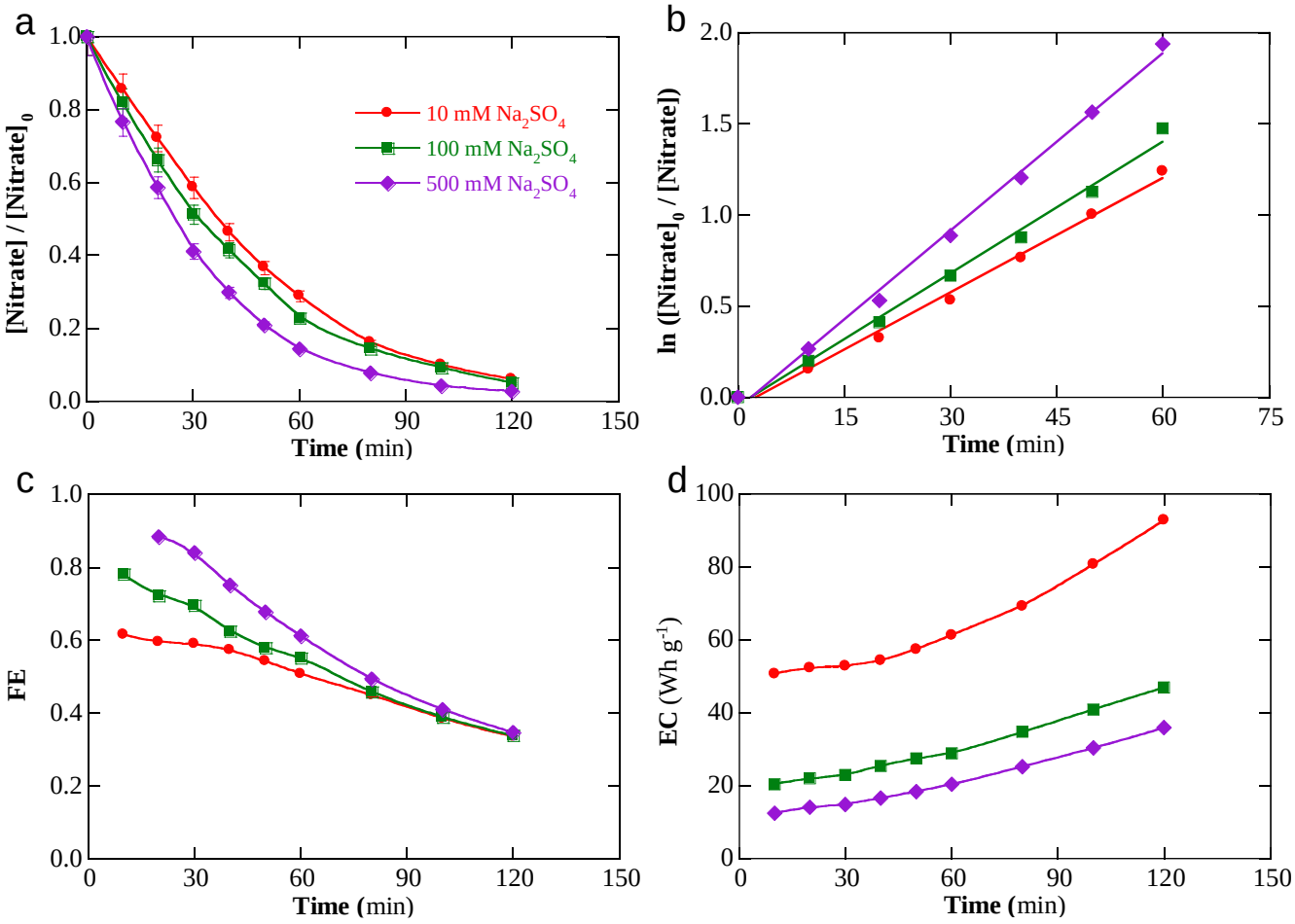
a
[Nitrate] / [Nitrate]0
Time (min)
10 mM Na2SO4
100 mM Na2SO4
500 mM Na2SO4
b
ln ([Nitrate]0 / [Nitrate])
Time (min)
c
FE
Time (min)
d
EC (Wh g-1)
Time (min)

Fig. 8

Table 1

First-order rate constant (k_1) determined from Fig. 4b with RCE at ω = 300 rpm, heterogeneous charge transfer constants (k_h) obtained from the Koutecky-Levich analysis with RDE from Fig. 2c, and *Da* values determined upon combination of Eqs. (13) and (16).

E_{cath} (V vs $Hg\|Hg_2SO_4$)	k_1 (10^{-4} s^{-1})	k_h (10^{-3} cm s^{-1})	*Da*
-1.60	n.d.	3.1	0.9
-1.65	1.9	3.7	1.1
-1.70	3.9	5.0	1.5
-1.75	n.d.	6.7	2.0
-1.80	6.4	8.1	2.4
-1.85	n.d.	10.8	3.2
-1.90	7.5	12.8	3.8
-2.20	7.7	n.d.	n.d.

Table 2

First-order rate constants (k_1) obtained from Fig. 5b at E_{cath} = -1.80 V, mass transport coefficient (k_m) obtained from Eq. (16), and dimensionless *Re*, *Sh* and *Da* numbers obtained from Eqs. (18) and (19) and (9), respectively.

ω (rpm)	*u (cm s^{-1})*	k_1 (10^{-4} s^{-1})	k_m (10^{-3} cm s^{-1})	*Re*	*Sh*	*Da*
100	19.9	4.5	2.0	8592	408	4.0
200	39.8	5.9	2.9	17184	576	2.8
300	59.7	6.6	3.4	25775	676	2.4
400	79.6	7.3	3.9	34367	785	2.1
500	99.5	7.8	4.3	42959	860	1.9